Internal loss in diode lasers with quantum well-dots

© A.E. Zhukov[1], A.M. Nadtochiy[1], N.V. Kryzhanovskaya[1], Yu.M. Shernyakov[2], N.Yu. Gordeev[2], A.A. Serin[2], S.A. Mintairov[2], N.A. Kalyuzhnyy[2], A.S. Payusov[2], G.O. Kornyshov[3], M.V. Maximov[3], Y. Wang[4]

[1] National Research University Higher School of Economics,
190008 St. Petersburg, Russia
[2] Ioffe Institute,
194021 St. Petersburg, Russia
[3] Alferov Federal State Budgetary Institution of Higher Education and Science Saint Petersburg National Research Academic University of the Russian Academy of Sciences,
194021 St. Petersburg, Russia
[4] Laser Institute, Shandong Academy of Sciences,
266100 Qingdao, P.R. China

E-mail: zhukale@gmail.com

Received May 4, 2022
Revised July 1, 2022
Accepted July 8, 2022

The internal loss at the lasing threshold were studied experimentally and numerically in laser cavities comprising dense arrays of InGaAs/GaAs quantum dots (quantum well-dots) as a function of the number of their planes and the output loss. Numerical values of the parameters were found that determine the free-carrier absorption in the active region and in the waveguiding layer. The optimal design of the laser diode was determined to achieve the highest external differential efficiency.

Keywords: diode lasers, semiconductor nanostructures, internal loss.

DOI: 10.21883/SC.2022.09.54138.9878

1. Introduction

Internal optical loss α_{in} is a crucial parameter of a semiconductor laser, since the ratio between it and output loss α_{out} sets the slope of the light-current curve. Long cavities (3 mm or longer [1]) with low output loss are normally used in power semiconductor lasers to reduce the thermal resistance. Ultralow internal loss providing an opportunity to maintain a high external differential efficiency and maximize the power conversion efficiency are vitally important for such lasers, since internal losses even as low as several cm^{-1} turn out to be unacceptable. Since the heterointerface roughness scattering of light in perfect epitaxial structures is negligible, modal internal absorption produces the greatest contribution to internal loss [2]. The use of a broadened waveguide allows one to suppress mode leakage into heavily doped cladding layers and thus reduce considerably the absorption of the optical mode by free carriers in claddings of laser heterostructures synthesized on both InP [3] and GaAs [4] substrates.

Thus, free-carrier absorption in the active region and the waveguide may play a significant part in the operation of modern semiconductor lasers, and the level of output losses affects the concentration of carriers at the lasing threshold and, consequently, the value of α_{in}. For example, the internal loss in [5] increased twofold when the cavity length was reduced from 3 mm to 150 μm, while the internal quantum efficiency remained within 10% error of its value determined for long samples. This demonstrates that an increase in internal loss (rather than a reduction in the internal quantum efficiency) is the factor that exerts a decisive influence on the variation of the external differential quantum efficiency on the cavity length. The waveguide filling and, consequently, internal loss may increase above the lasing threshold, thus inducing a nonthermal rollover of the light-current curve [6,7].

The optimization strategy for laser design (number of quantum-dimensional layers in the active region, waveguiding layer thickness, etc.) is evidently dependent on the ratio between internal losses attributable to absorption in the waveguiding layer and the active region. The emergence of new types of semiconductor active regions (specifically, ultradense arrays of quantum dots formed by non-Stranski–Krastanow growth regime, which are referred to as quantum well-dots, QWDs [8]) and new waveguiding structures (e.g., coupled large optical cavities [9]) makes the issue of examination of internal loss highly topical.

In the present study, we analyze the dependence of internal loss at the lasing threshold in QWD-based semiconductor lasers on the laser cavity length and the number of QWD planes experimentally and via modeling. It is demonstrated that the level of internal loss in long cavities and its growth in shorter waveguides (i.e., with an increase in output loss) are attributable to free-carrier absorption in the waveguide and the active region. The dominant mechanism of internal loss may be identified by analyzing the dependence of internal loss normalized to the number of QWD rows on the normalized threshold gain.

2. Experimental samples and research methods

Laser heterostructures were synthesized by metalorganic vapor-phase epitaxy on n^+ GaAs substrates. The active region features several planes of QWDs ($N_{QWD} = 1, 2, 5, 10$) separated by spacer GaAs layers with a thickness of 40 nm. QWDs were formed by deposition of eight monolayers of $In_{0.4}Ga_{0.6}As$. The use of substrates misoriented by 6° with respect to the (100) plane facilitated the formation of a dense island array. The active region was positioned at the center of an undoped waveguiding GaAs layer with a thickness of $\sim 0.8\,\mu$m cladded by $Al_{0.39}Ga_{0.61}As$ layers doped with n- and p-type impurities with a concentration of $7 \cdot 10^{17}\,cm^{-3}$.

Laser diodes with a wide stripe ($100\,\mu$m) with uncoated cleaved facets were fabricated. Cavity length L was varied from 4 mm to $100\,\mu$m, which corresponds to a range of variation of output loss $\alpha_{out} = L^{-1}\ln(R^{-1})$ from 3 to $120\,cm^{-1}$ (assuming that reflection coefficient $R = 0.3$). The samples were soldered onto copper heat sinks (p side down) are tested with thermal stabilization of the heat sink at 27°C under pulsed pumping (the pulse duration was $0.3\,\mu$s, and the repetition rate was 2 kHz). We believe that this helped avoid the effects of overheating of the active region (at least at current densities close to the lasing threshold). The light-current curves measured using a large-area calibrated Ge photodiode were used to determine the near-threshold external differential efficiency, which was then used to calculate (with the lasing wavelength taken into account) external differential quantum efficiency η_D.

The external differential quantum efficiency is specified by the ratio between radiation output losses and total losses. Its reciprocal value

$$(\eta_D)^{-1} = (\eta_i)^{-1}\left(\frac{\alpha_{out}}{\alpha_{in} + \alpha_{out}}\right)^{-1} = (\eta_i)^{-1}\left(1 + \frac{\alpha_{in}}{\ln(R^{-1})}L\right), \quad (1)$$

should vary linearly with cavity length if the other parameters remain unchanged. Here, η_i is the internal quantum efficiency of lasing, which was determined for the studied lasers by approximating the experimental values of η_D for long cavities ($L \geq 2$ mm) with (1). The approximation of dependence $(\eta_D)^{-1}-L$ also provided an opportunity to determine the level of internal loss for long lasers α_{in0}. The internal losses for shorter laser cavities were derived from the experimental values of η_D using expression (1) under the assumption that η_i remains constant. The total optical loss, which is equal to the modal gain of the active region at the lasing threshold, was then determined for each laser diode: $G_{th} = \alpha_{in} + \alpha_{out}$. Since the external differential quantum efficiency was determined based on the slope of a light-current curve near the lasing threshold, all values of internal losses considered here also correspond to the lasing threshold.

3. Experimental results

Figure 1 presents the experimental $(\eta_D)^{-1}-L$ dependences for laser structures with different numbers of QWD planes. It can be seen that these dependences are approximately linear for all structures with long cavities. An example approximation of experimental data for $N_{QWD} = 10$ with a linear function is represented by the dashed line. The values of η_i and α_{in0} derived via approximation for different numbers of QWD layers in the active region are presented in the inset of Fig. 1. It is evident that the internal quantum efficiency does not exhibit any regular dependence on N_{QWD} and remains within the range of 0.82 ± 0.03 in all laser structures. At the same time, α_{in0} increases approximately by $0.2\,cm^{-1}$ when a QWD row is added to the active region. This suggests that free carrier absorption in the active region is the factor that exerts a significant influence on α_{in0} in long lasers (i.e., in the case of low radiation output losses).

The reciprocal differential quantum efficiency decreases as the cavity gets shorter, reaches its minimum, which corresponds to the maximum external differential efficiency, and starts growing after that. This variation pattern is attributable to the fact that, in contrast to the absorption in cladding layers that feature a constant carrier concentration, internal losses found in (1) do change.

Figure 2 shows the dependences of internal loss for all structures on threshold current density J_{th}. It can be seen that the internal losses in all structures increase considerably in the region of high J_{th} (this also corresponds to greater

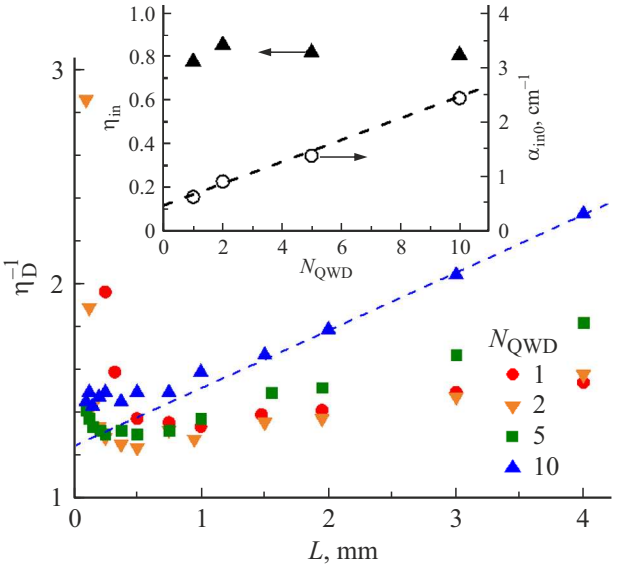

Figure 1. Dependences of experimental values of the reciprocal external differential efficiency on the cavity length (symbols) for lasers with different numbers of QWD planes and linear approximation for long cavities (dashed line). Dependences of the internal quantum efficiency (filled symbols) and internal loss in long cavities (open symbols) on the number of QWD planes are shown in the inset. (A color version of the figure is provided in the online version of the paper).

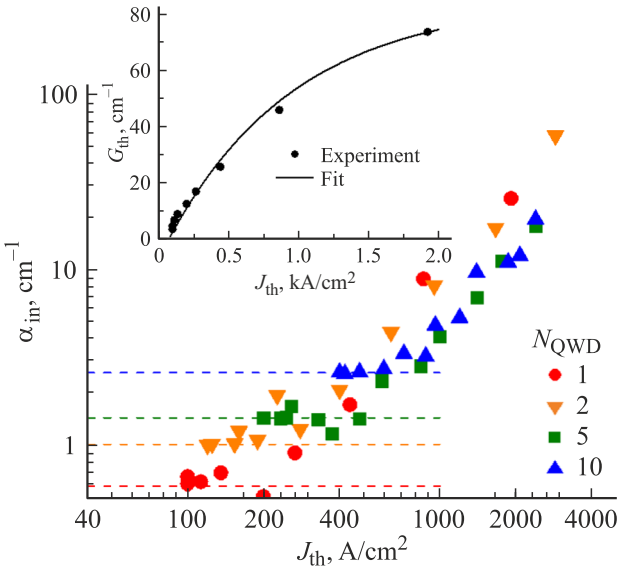

Figure 2. Dependences of the experimental values of internal loss on the threshold current density (symbols) for lasers with different numbers of QWD planes. Lines represent internal losses in long cavities. The relation between the threshold modal gain and the threshold current density ($N_{QWD} = 1$) is shown in the inset: symbols denote experimental data, while the curve is the result of approximation with expression (2).

losses at lasing threshold (G_{th}). The most pronounced increase in α_{in} ($> 100\,\text{cm}^{-1}$) is found in the structure with the smallest number of QWD planes in the active region. Note that the lasing wavelength in the shortest lasers ($L = 100 \ldots 200\,\mu\text{m}$) with $N_{QWD} = 1$ ceases to correspond to the ground-state optical transition of the active region with a wavelength around 1080 nm and shifts into the interval below 900 nm. This is indicative of significant filling of states (including those of the GaAs waveguide). These data were not used in the analysis.

The relation between threshold current density J_{th} and total optical loss determined for lasers of various length with a single QWD plane in the active region is shown in the inset of Fig. 2. Only the data corresponding to lasing through QWD states ($L > 200\,\mu\text{m}$) are presented. A satisfactory approximation of this dependence is provided by the following relation that was proposed earlier for the gain of QD lasers [10]:

$$G_{th} = G_{sat}\left(1 - \exp\left(-\chi\,\frac{J_{th} - J_0}{J_0}\right)\right), \qquad (2)$$

where $J_0 = 75\,\text{A/cm}^2$ is the current density needed to achieve population inversion, $\chi = 0.08$ is a parameter of the linear section of the dependence of gain on current density, and $G_{sat} = 85\,\text{cm}^{-1}$ is the maximum (saturated) gain corresponding to complete filling of the active region. The estimated value of G_{sat} is close to the maximum modal absorption ($70 \pm 15\,\text{cm}^{-1}$) obtained for a laser heterostructure of a similar design with a single QWD layer [11]. The saturated material gain of a single QWD layer was found to be equal to $1.5 \cdot 10^4\,\text{cm}^{-1}$ in [12]; with the calculated optical confinement factor of the active region taken into account, this yields an estimate of $55\,\text{cm}^{-1}$ for the saturated modal gain. In our view, a lower value of G_{sat} is found owing to the fact that the increase in internal loss in short cavities was neglected in [12].

Since the carrier concentration in claddings is fixed (in contrast to the carrier concentration in the active region and the waveguide), internal loss α_{clad} induced by absorption in these layers also remain constant. Thus, the obtained experimental data indicate that free-carrier absorption both in the active region (α_{act}) and in the waveguide (α_{WG}) plays a prominent part in the studied lasers. The corresponding components of internal loss are defined by fraction Γ of the optical mode in a given region of space, volumetric (cm^{-3}) concentrations of electrons (N) and holes (P), and absorption cross sections $\sigma_{N,P}$ for electrons and holes:

$$\alpha_{clad} = \Gamma_{clad}\left[N_{clad}\sigma_{clad\_N} + P_{clad}\sigma_{clad\_P}\right], \qquad (3a)$$

$$\alpha_{act} = N_{QWD}\Gamma_{act}\left[N_{act}(F_e)\sigma_{act\_N} + P_{act}(F_h)\sigma_{act\_P}\right], \qquad (3b)$$

$$\alpha_{WG} = \Gamma_{WG}\left[N_{WG}(F_e)\sigma_{WG\_N} + N_{WG}(F_h)\sigma_{WG\_P}\right]. \qquad (3c)$$

The position of quasi-Fermi levels of electrons F_e and holes F_h defines both the carrier concentrations in the active region and the waveguide and population inversion γ of states of the active region through which lasing is enacted ($\gamma = 1$ corresponds to the complete filling of states). An unambiguous relation between internal loss and the threshold modal gain is thus established:

$$G_{th} = N_{QWD}G_{sat}\,\gamma(F_e, F_h). \qquad (4)$$

We assume in the present case that saturated gain scales linearly with the number of QWD layers; the shift of side layers relative to the mode maximum and the probable nonuniformity of the distribution of carriers between different QWD layers at $N_{QWD} \geq 2$ are neglected.

It follows from (3) and (4) that an increase in the number of QWD planes at fixed values of F_e and F_h leads to a proportional enhancement of both gain and free-carrier absorption in the active region, while the absorption in the waveguide and the cladding remains unchanged. If the α_{act} component is dominant in internal loss, the dependences of normalized internal loss (α_{in}/N_{QWD}) on the normalized threshold gain (G_{th}/N_{QWD}) should be the same for all structures. The relation between α_{in}/N_{QWD} and G_{th}/N_{QWD} derived from experimental data is presented in Fig. 3.

It can be seen that the data for structures with different numbers of QWD rows in the active region do indeed agree fairly well in the region of relatively large loss ($G_{th}/N_{QWD} \gtrsim 15\,\text{cm}^{-1}$). If the $\alpha_{clad} + \alpha_{WG}$ component is dominant, relations (3) and (4) indicate that, as long as the normalized threshold gain remains the same, normalized internal loss in structures with a smaller number of QWD planes should exceed the ones in structures with a greater number of planes. This pattern is indeed observed in the region of relatively minor normalized loss.

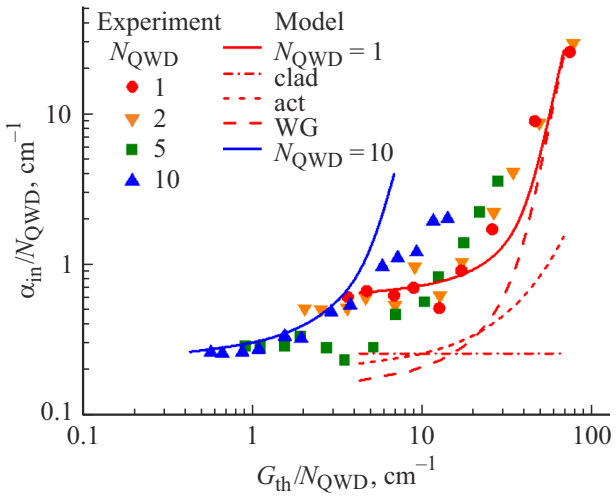

Figure 3. Relation between normalized internal loss and the normalized threshold gain for lasers with different numbers of QWD planes: symbols represent experimental data, and curves correspond to the results of modeling.

4. Simulation

It follows from the analysis of experimental data that internal loss in QWD-based lasers have a complex dependence on the number of planes and the threshold gain. In order to optimize the laser design and maximize the external differential efficiency, we modeled the absorption of light in the active region and the waveguide. The following 2D and 3D densities of states were used for the corresponding regions of the laser structure [13]:

$$\rho_{act}(E) = \frac{m}{d_{act}\pi\hbar^2}\,\theta(E), \tag{5a}$$

$$\rho_{WG}(E) = \frac{1}{2\pi^2}\left(\frac{2m}{\hbar^2}\right)^{3/2}\sqrt{E-\Delta}. \tag{5b}$$

Here, m is the effective mass of electrons or heavy holes, d_{act} is the effective thickness of the active region layer, and Δ is the energy of the electron (hole) level localization in the active region with respect to the edge of the conduction band (valence band) of the waveguide. Although QWDs are not entirely equivalent to a two-dimensional quantum well, a weak energy dependence of the photoresponse signal for electrons–heavy holes transitions [11] allows one to use step function $\theta(E)$ as a first approximation to the model density of states.

The overall electron and hole localization energy was estimated as 276 meV based on the difference between the band gap of the GaAs waveguide (1424 meV) and the energy of the ground-state optical QWD transition (its wavelength is 1.08 μm). The ratio of localization energies for electrons Δ_e and holes Δ_h was set arbitrarily to 0.5 : 0.5. The position of quasi-Fermi levels of holes F_h for a certain position of Fermi quasi-level of electrons F_e was determined using the electroneutrality condition. Saturated material gain per a single QWD layer was assumed, in accordance with the experimental estimate, to be equal to 85 cm^{-1}. Coefficients σ_N and σ_P in all layers were taken equal to $4 \cdot 10^{-18}$ and $12 \cdot 10^{-18}$ cm^2 [14], and the effective masses were 0.063 and 0.51 for electrons and heavy holes, respectively [15]. The calculation of optical confinement factors performed for the fundamental mode in the laser structure with $N_{QWD} = 1$ yielded $\Gamma_{clad} = 2.7\%$ (in each cladding), $\Gamma_{act} = 0.36\%$, and $\Gamma_{WG} = 94.2\%$. QWDs were substituted with a two-dimensional layer with thickness $d_{act} = 2.4$ nm in the calculation of Γ_{act}. Note that d_{act} is also found in the denominator of (5a) and, in accordance with (3b), does not affect the calculated value of α_{act}. With the above parameters, the calculated value of internal loss for a near-zero population inversion is 0.71 cm^{-1}, while the experimental value is $\alpha_{in0} = 0.61$ cm^{-1}. In order to bring the calculated absorption values closer to the experimental estimates, we corrected coefficients σ by a factor of 0.61/0.71 in subsequent calculations.

The calculated absorption in the waveguide and a single QWD layer in laser diodes with the maximum length is 0.15 and 0.2 cm^{-1}, respectively, and the absorption in claddings is 0.26 cm^{-1}. In line with experimental data (see the inset of Fig. 1), the absorption in the active region increases by 0.2 cm^{-1} following the addition of one QWD plane. The calculated normalized internal loss is represented by curves in Fig. 3. To avoid overloading the figure, only the results for two limit cases ($N_{QWD} = 1$ and 10) are presented. The modeling results are close to the experimental data in magnitude; the sole exception is the region of high G_{th}/N_{QWD} values for a large number of QWD planes. The probable reason for this deviation is nonuniform filing of QWD layers with carriers: the concentration of holes (electrons) may decrease with distance between the plane and the p- (n-) cladding. This, in turn, implies that saturated gain increases with number of planes slower than $N_{QWD}G_{sat}$; therefore, we underestimate the value of G_{th}/N_{QWD} for multilayer lasers in calculations.

The individual components of internal loss are also shown for $N_{QWD} = 1$. In general, the results of calculations represent accurately the major features of experimental dependences, such as the reduction of normalized internal loss in the region of low normalized threshold gain values and their increase in the region of high normalized threshold gain values in lasers with a large number of QWD planes in the active region. The simulation results demonstrate that a rapid growth of internal loss with increasing G_{th}/N_{QWD} is caused by a sharp increase in the carrier concentration in the waveguide at a high level of population inversion in the active region.

The developed model allows one to formulate a strategy for optimization of the active region design. Let us discuss this using the example of selecting the optimum number of planes needed to maximize the external differential quantum efficiency as a function of radiation output losses. The corresponding dependence is shown in Fig. 4. It can be seen that the heterostructure with a single QWD layer in

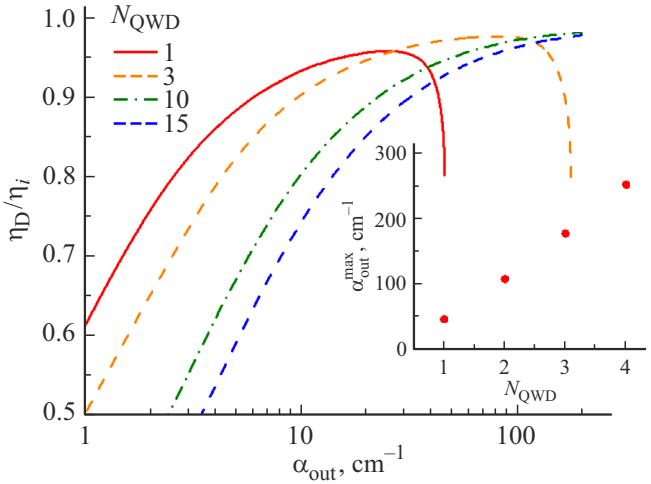

Figure 4. Calculated dependence of the normalized external differential quantum efficiency on output loss for lasers with different numbers of QWD planes. Dependence of the maximum allowed output loss on the number of planes is shown in the inset.

the active region provides the highest η_D at low levels of radiation output loss (up to $\alpha_{out} \approx 20\,cm^{-1}$); at α_{out} around $50\,cm^{-1}$, $N_{QWD} = 3$ is the optimum value. The optimum number of N_{QWD} increases with α_{out}. It is also worth noting that, since internal loss increase rapidly with increasing population, they also needs to be taken into account together with saturation of optical gain in the determination of the maximum magnitude of output loss α_{out}^{max} at which lasing is possible with a given number of QWD planes in the active region. When α_{out} approaches α_{out}^{max}, the external differential efficiency starts decreasing rapidly. The dependence of α_{out}^{max} on the number of QWD planes is shown in the inset of Fig. 4 for $N_{QWD} \leq 4$. The values of α_{out}^{max} for larger numbers of planes are so high that they become irrelevant to the laser design selection.

5. Conclusion

Thus, the external differential efficiency of lasers with different numbers of quantum well-dot planes in the active region was examined. It was found by analyzing the dependence of the reciprocal differential efficiency on the laser cavity length that the internal loss at the lasing threshold increase as a cavity gets shorter. The magnitudes of this loss and the threshold modal gain were determined. A satisfactory approximation of the experimental dependences may be obtained under the assumption that internal loss are defined both by free-carrier absorption in the active region, which scales with the number of QWD planes, and by the waveguide absorption. In long cavities, these types of absorption are characterized by the values of about $0.2\,cm^{-1}$ per a single QWD plane and approximately $0.15\,cm^{-1}$. The increase in loss in short cavities is attributable to the growth of population of both the active region and the waveguide; at high levels of output loss, the waveguide absorption is dominant. The rapid growth of internal loss sets a certain maximum level of output loss at which lasing is feasible (with the maximum possible modal gain taken into account). When the output loss increases, the optimum number of QWD planes providing the highest external differential efficiency increases from 1 to 3.

Funding

This work was supported by project „New Optical Waveguides and Cavities for Edge- and Vertically-Emitting Laser Diodes“ (FTI-LISDAS). Modeling was performed with support from the Fundamental Research Program of the HSE University. This study was supported in part by the Ministry of Science and Higher Education of the Russian Federation, project 0791-2020-0002.

Conflict of interest

The authors declare that they have no conflict of interest.

References

[1] T. Kaul, G. Erbert, A. Maassdorf, S. Knigge, P. Crump. Semicond. Sci. Technol., **33**, 035005 (2018). DOI: 10.1088/1361-6641/aaa221
[2] L.A. Coldren, S.W. Corzine, M.L. Masanovic. In: *Diode Lasers and Photonic Integrated Circuits,* 2nd edn (Wiley, 2012) p. 570.
[3] D. Garbuzov, L. Xu, S. Forrest, R. Menna, R. Martinelli, J. Connolly. Electron. Lett., **32** (18), 1717 (1996). DOI: 10.1049/el:19961098
[4] A. Al-Muhanna, L.J. Mawst, D. Botez, D.Z. Garbuzov, R.U. Martinelli, J.C. Connolly. Appl. Phys. Lett., **71** (9), 1142 (1997). DOI: 10.1063/1.119847
[5] J. Piprek, P. Abraham, J.E. Bower. IEEE J. Select. Top. Quant. Electron., **5** (3), 643 (1999). DOI: 10.1109/2944.788430
[6] L.V. Asryan. Appl. Phys. Lett., **88**, 073107 (2006). DOI: 10.1063/1.2174103
[7] Z.N. Sokolova, D.A. Veselov, N.A. Pikhtin, I.S. Tarasov, L.V. Asryan. Semiconductors, **51** (7), 959 (2017). DOI: 10.21883/FTP.2017.07.44661.8522
[8] M.V. Maximov, A.M. Nadtochiy, S.A. Mintairov, N.A. Kalyuzhnyy, N.V. Kryzhanovskaya, E.I. Moiseev, N.Yu. Gordeev, Yu.M. Shernyakov, A.S. Payusov, F.I. Zubov, V.N. Nevedomskiy, S.S. Rouvimov, A.E. Zhukov. Appl. Sci., **10** (3), 1038 (2020). DOI: 10.3390/app10031038
[9] N.Yu. Gordeev, A.S. Payusov, Yu.M. Shernyakov, S.A. Mintairov, N.A. Kalyuzhnyy, M.M. Kulagina, M.V. Maximov. Optics Lett., **40** (9), 2150 (2015). DOI: 10.1364/OL.40.002150
[10] A.E. Zhukov, A.R. Kovsh, V.M. Ustinov, A.Yu. Egorov, N.N. Ledentsov, A.F. Tsatsul'nikov, M.V. Maximov, Yu.M. Shernyakov, V.I. Kopchatov, A.V. Lunev, P.S. Kop'ev, D. Bimberg, Zh.I. Alferov. Semicond. Sci. Technol., **14** (1), 118 (1999). DOI: 10.1088/0268-1242/14/1/020

[11] A.M. Nadtochiy, N.Yu. Gordeev, A.A. Kharchenko, S.A. Mintairov, N.A. Kalyuzhnyy, Yu.S. Berdnikov, Yu.M. Shernyakov, M.V. Maximov, A.E. Zhukov. J. Lightwave Technol., **39** (23), 7479 (2021). DOI: 10.1109/JLT.2021.3116261
[12] N.Yu. Gordeev, M.V. Maximov, A.S. Payusov, A.A. Serin, Yu.M. Shernyakov, S.A. Mintairov, N.A. Kalyuzhnyy, A.M. Nadtochiy, A.E. Zhukov. Semicond. Sci. Technol., **36**, 015008 (2021). DOI: 10.1088/1361-6641/abc51d
[13] C.W. Shong, S.C. Haur, A.T.S. Wee. In: *Science at the Nanoscale. An Introductory Textbook* (Pan Stanford Publishing, 2010) p. 109.
[14] K.H. Hasler, H. Wenzel, P. Crump, S. Knigge, A. Maasdorf, R. Platz, R. Staske, G. Erbert. Semicond. Sci. Technol., **29**, 045010 (2014). DOI:10.1088/0268-1242/29/4/045010
[15] I. Vurgaftman, J.R. Meyer, L.R. Ram-Mohan. J. Appl. Phys., **89** (11), 5815 (2001). DOI: 10.1063/1.1368156